# UC San Diego
## UC San Diego Electronic Theses and Dissertations

**Title**
Analysis of the Projections of Melanopsin Expressing Retinal Ganglion Cells to the SCN

**Permalink**
https://escholarship.org/uc/item/1jb2g338

**Author**
Shoghi, Azarin

**Publication Date**
2018

Peer reviewed|Thesis/dissertation

UNIVERSITY OF CALIFORNIA SAN DIEGO


Analysis of the Projections of Melanopsin Expressing Retinal Ganglion Cells to the SCN


A Thesis submitted in partial satisfaction of the requirements

for the degree Master of Science


in


Biology


by


Azarin Shoghi


Committee in charge:

    Professor Satchidananda Panda, Chair
    Professor Nickolas Spitzer, Co-Chair
    Professor Brenda Bloodgood
    Professor Shelley Halpain

2018

The Thesis of Azarin Shoghi is approved, and it is acceptable in quality and form for publication on microfilm and electronically:

_____

_____

_____

Co-Chair

_____

Chair

University of California San Diego

2018

# DEDICATION

I would like to dedicate this thesis to my mother who has always supported me and has never doubted my abilities to attain success.

# TABLE OF CONTENTS

LIST OF FIGURES

ABSTRACT OF THE THESIS


Analysis of the Projections of Melanopsin Expressing Retinal Ganglion Cells to the SCN


by


Azarin Shoghi


Master of Science in Biology

University of California San Diego, 2018

Professor Satchidananda Panda, Chair

Professor Nicholas Spitzer, Co-Chair


The suprachiasmatic nucleus (SCN) of the hypothalamus is known as the master clock, which controls mammalian circadian rhythms. Located in the brain above the optic chiasm, the SCN entrains to daily environmental light cycles via innervations from the retina. Intrinsically photosensitive retinal ganglion cells (mRGCs), which express the photopigment melanopsin, send axonal projections down the retinohypothalamic tract (RHT). Each mRGC communicates

with neurons in the SCN via boutons, small swellings along its axonal length filled with vesicles containing neuropeptides. The SCN consists of two morphologically distinct regions where synaptic connections of the RHT deliver light information: the core and the shell. In this study we reconstructed the connectome of the mRGC network in the shell and core regions of the SCN using the electron microscopy tag APEX2, and characterized differences in the structures of the two SCN regions using IMOD software to reconstruct 3D images of neurons. Quantification of synaptic strength between mRGCs and the SCN was evaluated by measuring the bouton density and average volume of mRGC synapses. We found that the average bouton volume of the mRGC contacts in the SCN shell are significantly larger than those in the SCN core however, mRGCs make fewer connections in the shell than the core. Reconstruction of the neuronal connections is necessary for the understanding of the flow of information from the retina to the SCN, and this understanding may aid and expedite the development of therapies targeting disruptions in the mammalian circadian rhythms.

**Circadian Rhythms**

Mammalian circadian rhythms are created by an internal body clock that regulates and synchronizes behavioral patterns such as eating and sleeping (Takahashi et al. 2008). The human circadian clock is synchronized to the 24-hour day and night cycle, which is dependent on the rising and setting of the sun. To demonstrate that humans possess an intrinsic circadian clock irrespective of outside stimuli, Jürgen Aschoff performed an experiment in which college students were kept in isolation from all external stimuli and their eating and sleeping patterns were monitored (Aschoff 1965). The study showed that the students had regular eating and sleeping patterns, regardless of whether they had environmental light cues to guide them in time. Later it was discovered that specialized cells within the suprachiasmatic nucleus (SCN) of the hypothalamus generate and maintain a cyclic rhythm that coincides with the length of a day on Earth (Herzog et al. 1998). The SCN is a body clock that regulates behavior such as sleep, metabolism, and hormonal regulations, making daily physiological and behavioral functions dependent on this clock. Disruptions in the function of circadian rhythms are linked to sleep related diseases and other diseases such as diabetes and cancer (Takahashi et al. 2008). Hence, understanding of the workings of the body clock is of importance due to its connection to many different bodily functions.

**SCN Functions**

The master clock of the body in the SCN (Abrahamson and Moore 2001) has three main functions that support its role as a timekeeper. Most importantly, the SCN contains auto-rhythmic cells that cycle in the absence of external stimuli, maintaining an intrinsic rhythm which other bodily systems can follow (Welsh et al. 1995; Aton and Herzog 2005). SCN neurons

are heavily interconnected and rely on their robust network of synaptic connections and cellular communication to maintain their synchronized rhythms (Hastings and Herzog 2004). While some cells of the SCN are hard-wired to rhythmically express certain genes, photic information delivered from the retina functions to synchronize these innate rhythms to the environmental day and night cycle, also known as entrainment (L. P. Morin and Allen 2006). The SCN regulates clocks of the rest of the body to ensure that time-dependent activities are completed in a precisely coordinated fashion (Gachon et al. 2004). The SCN drives the rhythms of other tissues in such a manner that without the SCN, the clock of other organs either weakens or desynchronizes completely (Kornmann et al. 2007), exemplifying the necessity of this relatively small region of the hypothalamus.

**SCN Structure**

The location of the SCN above the optic chiasm allows it to receive direct light information from the eye, through the retinohypothalamic tract (RHT) (Lawrence P Morin 2013). The RHT consists of a set of neuronal axons that project from the retina to multiple brain regions including the SCN (Moore 1995). In earlier studies, it was discovered that the axons running through the RHT are vital for entrainment, whereas other axons beyond the optic chiasm were only required for visualization and not entrainment. The SCN also receives innervation from different brain regions, including the raphe nucleus, the intergeniculate leaflet and other hypothalamic regions (Moore and Card 1994). Each unilateral structure of the SCN consists of 8,000-10,000 neurons with distinct morphology, the majority of them being multipolar or bipolar (van den Pol 1980).

**SCN Core and Shell**

The bilateral structure of the SCN contains two sub-regions: the ventrolateral core, and the dorsomedial shell (Abrahamson and Moore 2001). These two divisions are defined as such based on the structural anatomy of the SCN neurons in these regions and their distinct function (Nakamura et al. 2001). A distinct boundary does not exist between the two regions of the SCN; the core and the shell regions are defined by the neuropeptides they release. Each region of the SCN is responsible for the control of a different aspect of the circadian rhythm and are composed of spatially-specific neurons (Moore et al. 2002). Noguchi and colleagues tested the rhythms of the SCN core and SCN shell separately, then compared the rhythms of the two regions to a control animal with an intact core and shell region. They discovered that the shell region of the SCN contains neurons that have a slower rhythm than the core, whereas the rhythm of the core region was the same as a control animal with an intact SCN. Hence, it was shown that the core region was responsible for generating rhythms which then travel to the shell region, and further, to the body (Noguchi et al. 2004). These findings demonstrate the functional differences between the two regions of the SCN.

The functions of the core and shell may be different due to the hormones that they express, which are region specific. The core expresses a neuropeptide called vasoactive intestinal peptide (VIP) (Abrahamson and Moore 2001), whereas the shell is known to express the neuropeptide arginine vasopressin (AVP) (Abrahamson and Moore 2001). Additionally, the core of the SCN receives axonal projections directly from the retina and projects this information to the shell region (Abrahamson and Moore 2001), but the shell does not send many neuronal axons back to the core (Leak et al. 1999). The quantity of projections from each region, as well as their

specific expression of neuropeptides is important in the control of circadian rhythms, and accounts for the differences in the functions of the two SCN regions (Mieda et al. 2015).

**mRGCs**

In order for the human body to entrain to the day and night cycle, the SCN receives projections from the retina. Rods and cones are photosensitive cells that detect light information in the retina and send it to the brain for visual interpretation (Hattar 2002). Aside from rods and cones, a subset of retinal ganglion cells (RGCs) are also located in the retina that send light information to the SCN for circadian rhythm entrainment. These cells express the photo-pigment melanopsin and are intrinsically photosensitive however, they are not involved in visual perception (Hattar 2002). To support the notion that rods and cones are not involved in circadian rhythm regulation, Kofuji and colleagues ablated rods and cones in mice and monitored the activity of these visually impaired mice. They found that the mice continued to have intact circadian rhythms, indicating the presence of an alternate system for communicating light information to the brain. They performed another experiment, where they knocked out only the intrinsically photosensitive retinal ganglion cells (mRGCs) of mice, leaving rods and cones intact. Mice with non-functional mRGCs retained their image forming vision, but they did not entrain to day and night cycle (Kofuji et al. 2016), providing support to the notion that mRGCs are involved in the transmission of non-image forming photic information to the SCN.

Structural analysis has demonstrated that there are five different types of mRGCs, M1-M5, with each type projecting to a different brain region. The M1 mRGC projects to the SCN (Schmidt et al. 2011), and is known to control the pupillary light reflex (PLR) (Berson et al. 2002). Beyond the type of mRGC, little is known about their specific connectivity within the SCN (Ecker et al. 2010).

Studies indicate that mRGCs communicate with SCN neurons through the release of the neurotransmitters glutamate and pituitary adenylate cyclase-activating polypeptide (PACAP) (Welsh et al. 2010), with the release of PACAP enhancing the effects of glutamate. When stimulated with light, a wave of depolarization runs down the mRGC axon, which results in neurotransmitter release. Glutamate is released into the synaptic cleft where it may bind AMPA and NMDA receptors on SCN neurons, then through a cascade of post synaptic activities intracellular calcium levels increase. The change of calcium levels will trigger activation of gene expression of the clock genes, thus their movement forward or backward within time to adjust to the light information received (Welsh 2007).

In this study, we work to understand the connectivity of mRGCs in the SCN core and shell through observation of bouton size, number of synapses per bouton, axon shape and length. We also look at structural differences between the SCN core and shell, as understanding structural morphology will take us a step closer to understanding the functions of the two regions.

**Electron Microscopy**

Due to the small size and the difficulty of visualizing the axons and synaptic connections within the SCN, electron microscopy (EM) was our chosen mode of visualization. Previously, neuronal connections were visualized using light microscopy (LM). While LM is effective at locating and visualizing neuronal arbors unfortunately, LM is limited to resolution of 200 nm and synaptic cleft diameters are on the order of 0.9 nm (Guldner 1976). To overcome this limitation, electron microscopy (EM) can be used to resolve images up to 0.2 nm, a significantly higher resolution than that offered by LM. Therefore, using EM for visualization of the mRGC projections in the SCN is preferred, as this method will allow us to resolve mRGC axons and dendrites in addition to the synaptic cleft and the synaptic vesicles at the site of a synapse.

**Serial Block-Face Electron Microscopy**

In addition, serial block face scanning electron microscopy (SBEM) allows us to slice the mouse brain into very thin sections and image the complex structural anatomy of the neurons in the SCN. SBEM is preferred for use because thin section of the brain is imaged, which can then be stacked using computer software to reconstruct a 3D image of the neuronal network within the SCN (Denk and Horstmann 2004).

**APEX2**

The visualization of a specific protein or cell type under electron microscopy proves a difficult task. Therefore, an electron microscopy genetic tag was necessary to visualize mRGC axons and their synaptic connections that projected in the SCN. Different EM tags which function similar to green fluorescent proteins in LM (Shu et al. 2011) are used to keep track of neuronal axons during SBEM . In this project we used APEX2, a peroxidase which catalyzes the polymerization of 3,3-diaminobenzidine (DAB) under electron microscopy. DAB localizes $OsO_4$ which under electron microscopy gives a dark contrast (Lam et al. 2014). This EM tag proved efficient at locating mRGC axons and axon terminals in the SCN section.

Understanding structural anatomy of a brain region will lead to a better understanding of the function of the region. For example, it was not known that the master clock of the body was contained within the SCN until the RHT was followed from the retina (Moore 1995). Similarly, discoveries about structural anatomy and connection between the neurons of the RHT and SCN will lead to a deeper understanding of the underlying physiological functions controlled by the master clock. Studying axonal projections in the brain tends to be difficult due to visualization limitations however, it is important to study these connections due to their potential implications

for mammalian circadian rhythm pathologies. Therefore, this study focused on tracing axons from the RHT in the SCN using the electron microscopy tag APEX2 to label the mRGCs, and SBEM to visualize thin sections and resolve images in the order of 0.9nm, to recreate a map of the connections in the SCN core and shell. This map may help understand the connectivity of mRGCs to the SCN. With this information we can evaluate connective differences between the core and the shell of the SCN. By bettering our understanding of mRGC connections, we can address circadian rhythm pathologies and related diseases using mRGC targeted therapies.

METHODS

*Mice*

Male $Opn4^{Cre/+}$ mice older than 8 weeks used.

*Vector Construction*

A farnesyl sequence was cloned into the 3' end of the APEX2 construct and was inserted in an inverted orientation between the lox sites in an AAV-DIO vector to create AAV-DIO-Mito-V5-APEX2-f and AAV2-DIO-tdTomato-f was produced by the Salk Gene Transfer, Targeting and Therapeutics Viral Vector Core Facility at titers of 1.09 x $10^{11}$ TU/ml and 9.41x$10^{11}$ TU/ml, respectively.

*Vector Injection*

To express APEX2 and tdTomato mRGCs, 3 µl of AAV2-EF1α-DIO-APEX2 and 0.3 µl of AAV2-EF1α-DIO-tdTomato was injected into both eyes of $Opn4^{Cre/+}$ mice between the ages of 8 weeks and 6 months old.

*SBEM Staining and Imaging*

Tissue was prepared for SBEM as previously described (Deerinck et al., 2010). The retina and brain volumes were collected in 2.0 kV accelerating voltages, with a raster size of 10k × 10k and pixel dwell time of 2 µs. The pixel sizes were 7 nm, depending on the raster size and section thickness was 50 nm. Before each volume was collected, a low magnification (~500×) image was collected of the block face to confirm the anatomical location of the volume based on tissue landmarks, such as the RGC, SCN, and the OPN. Once a volume was collected, the

8

histograms for the slices throughout the volume stack were normalized to correct for drift in image intensity during acquisition. Digital micrograph files (.dm4) were normalized using Digital Micrograph and then converted to MRC format. The stacks were converted to eight bit, mosaics were stitched, and manual or semi-automated tracing was used to calculate volume for reconstruction and analysis.

### *Three-Dimensional Reconstruction and Analysis*

To analyze these datasets, we used the publicly available software package IMOD, specifically developed for the visualization and analysis of EM datasets in three dimensions (Kremer et al., 1996; http://bio3d.colorado.edu/imod/). Cross-sectional contours were manually traced for consecutive data slices in the *z* dimension to determine the boundaries of user-defined objects. For some objects, contours were traced in every other data slice in the *z* dimension. These contour profiles were used for three-dimensional volumetric reconstruction of APEX2 expressed mRGC cell body, axons and boutons. Boutons are defined as an axon swelling containing a continuous stretch of synaptic vesicles and/or mitochondria. Volume measurement begins and ends with the vesicles and/or mitochondria. For quantification of mRGC bouton volume, surface area, postsynaptic spiny dendrite invaginations, and mitochondria, APEX2 labeled boutons were unbiasedly sampled at the 25 intersection points of a 5 x 5 grid overlaid on the image stack. Either the first bouton in the stack to intersect with a grid point or the closest bouton to it was sampled. Those boutons were then manually segmented, and their volume was computed. Subsequently, the number of post-synaptic spiny dendritic protrusions that invaginated the bouton (termed spine invaginations) and the number of mitochondria per bouton were also quantified. For SCN core and shell mRGC input characterization, the 20 most centrally located neurons were manually segmented from SCN core and shell. All mRGC axons synapsing

with each of the segmented neurons was also segmented. The dendrite and axon length were measured. Total synaptic boutons per neuron, synaptic boutons per dendritic length and boutons per axon length were calculated.

*Manual segmentation*

*Three-dimensional reconstruction of mRGC axons and boutons:*

Created a 5 x 5 grid that resulted in 25 boxes. Out of the 25 boxes, 9 were selected from which manual segmentation would be done. From these 9 boxes, all of the visible mRGC boutons were selected and their axons traced until it either reached the end of the data set or it reached the edge of the box that was being traced from. The boutons in the boxes were also segmented every 2 z-steps. Using *imodmesh*, the segmentations for the boutons were meshed and their volumes calculated. The total volumes were then averaged. In addition, the density of mRGC boutons were calculated by counting the total number of mRGCs and dividing by the combined volume of the 9 boxes from which the tracing was done.

*Axon length:*

APEX2 labeled axons were found by first finding a bouton having darkly labeled mitochondria. The axons connected to this bouton were traced until another bouton was reached. The second bouton connected with a single axon was analyzed to decide whether the mitochondria was darkly labeled. This allowed for the identification of mRGC boutons and their axons. A new open contour object was made for each axon and individual consecutive points of a single open contour were placed in the center of APEX2-labeled axon cross-sections starting from the first slice in an image volume until the last slice in an image volume. If an axon branched, a new open contour was made for that axon object and another set of consecutive

10

points laid down for the branch. This was repeated until the entire axon was represented by an open contour skeleton line created from consecutive points. *Imodinfo* returned the length of all lines in the object.

### *Synapse quantification:*

For identification of synapses, we looked for areas of the axon that were swollen to a diameter at least twice as large as the average diameter of the axon. Our criteria for a swelling to be considered a synaptic bouton included at least two of the following: presence of a post-synaptic density in the cell directly contacting the swelling, presence of at least one mitochondria, or evidence of synaptic vesicles in the vicinity of the synapse. In order to count the number of synaptic boutons, each image volume was deconstructed into a 5 x 5 grid and the APEX2-labeled boutons in every other square column was counted. The contours that make up each bouton were traced out and meshed with *imodmesh* to determine bouton volume.

### *Grid-based selection scheme of mRGC boutons:*

A random set of 50 mRGC boutons were selected from the intersection points of a 5 x 5 grid that created 25 intersection points of IMOD. Going through the image stacks, the first labeled bouton to intersect with the grid point at select z-steps of 100, 200 and 400, or the closest bouton to it, was sampled. Subsequently, these boutons were back-traced to the limit of the volume to yield a segment of axon and more boutons. This allowed for a comprehensive and unbiased sampling of the tissue.

### Three-dimensional reconstruction of SCN core and shell neurons:

About 20-30 SCN neurons were selected from the middle section of the selected volume using IMOD. The neurons were observed to ensure that their soma was completely within our data set. The central neurons were selected in order to ensure that as much of their dendrites and axons and neuronal processes were captured within our data set as possible. Each soma, its dendrites and its axons were segmented using a separate contour, producing a separate color. Individual neurons were then meshed and using *imodmesh* to reveal their shape and structure in a 3D model view. Additionally, the meshing process allowed for the calculation of the neuron volume and diameter.

### Segmentation of myelinated axons:

For the segmentation of myelinated axons, we created a 5 x 5 grid and started at the lowest z-step in the data set and looked for axons with a thick dark myelin around them. These axons were traced using open contour to obtain an estimate of their length and branching pattern. This process was done until all the area in the volume sets of the SCN core and shell were covered.

### Counting of nuclei, astrocytes, stigmoid bodies:

To count the nuclei, astrocytes, and stigmoid bodies in the two data sets, a 5 x 5 grid was created. The entirety of the data set was scanned in a systematic way by starting from one corner and going through all the created grids and marking each of the nuclei, astrocyte, and stigmoid bodies with a different color. To determine the density of the SCN neurons in each of the SCN core and shell, individual SCN nuclei were counted in each section and the numbers divided by the respective region volume. A criterion was made so that nuclei that were completely within

our data set were labeled with a single color and called 100% nuclei. If a neuron's nuclei were

more than 50% within our data set, it was labeled with another color and those were counted

separately. If a neuron's nuclei were less than 50% within our data set it was labeled with a third

color and counted. To ensure that all of the areas of the data set were covered, a 5 x 5 grid was

created and nuclei search was done from the beginning of the section till the end in each grid

until all the grids were covered.

RESULTS

**mRGCs make more connections in the ventral SCN**

To begin, we sought to determine the morphological differences of cells that innervate

the core and shell regions of the SCN. Bouton volume and the density of mRGCs in dorsal and

ventral regions of the SCN were compared. We created a 5 x 5 grid and selected 9 out of 25 grids

in which all the mRGC boutons in those columns were traced. We found and traced 1064

boutons from the ventral SCN and 678 boutons from the dorsal SCN from a single adult male

mouse. The boutons were recreated into a 3D image using the computer software IMOD. The 3D

images were used to measure bouton volume. The average bouton volume calculated from the

ventral region of the SCN was 0.71 $\mu m^3$; and that calculated from the dorsal region was 0.84

$\mu m^3$ (Fig. 1c). Average bouton volume in the dorsal region is significantly larger than that of the

ventral (t Stat= 4.96; df= 1226; p= $8.0 \times 10^{-07}$). Additionally, the density of the boutons was

determined. The density was calculated by counting the total number of boutons in each of the

dorsal and ventral SCN and dividing this count by the total volume. The bouton density in the

ventral of the SCN (n= 1064 boutons) was 17.26 boutons per 1000 $\mu m^3$ and that in the dorsal

(n=678 boutons) was 14.81 boutons per 1000 $\mu m^3$ (Fig. 1d). The ventral region of the SCN

received more synaptic boutons compared to the dorsal region, whereas the dorsal received

larger synaptic boutons.

**Morphology of mRGC axons innervating the ventral and dorsal SCN**

For a comparison between the mRGC axon morphology of the ventral and dorsal SCN,

fifty randomly selected mRGC axons were traced and their boutons marked. The mRGCs were

randomly selected based on a 5x5 grid. The first mRGC bouton to contact a grid intersection at a

14

predefined z-step, would be selected. We calculated the number of boutons per length of axon

per mRGC axon and took an average for the ventral and dorsal regions of the SCN. On average,

there are about 9.4 boutons per 100 µm of axon length in the ventral SCN and 10.9 boutons per

100 µm in the dorsal SCN (Fig. 2b). A student's t-test indicated no significant difference

between the bouton distribution in the two regions of the SCN. Additionally, percentage of

mRGC axons in each region that contained a branch point was calculated to determine the

branch pattern of the axons. In the ventral region, 34 axons out of a total of 50 counted had a

branch point, and those of the SCN dorsal had 44 axons resulting in a branch points out of the 50

sampled axons (Fig. 2c). Performed a student's t-test and the results were not statistically

significant. Furthermore, mRGC axonal length in the dorsal and ventral SCN was calculated. In

the ventral SCN, mRGC axons are on average 42 µm in length and those in the dorsal SCN are

about 40 µm in length (Fig. 2d).

**Dorsal SCN is denser with neurons compared to the ventral SCN**

Individual nuclei that belong to SCN neurons were counted in each of the dorsal and

ventral SCN. The raw count of the nuclei obtained were divided by the respective volume of the

SCN region and the number was multiplied by 100,000 for a better comparison of the numbers.

For the nuclei that were 100% within our data set, we observed that the ventral SCN contained

22 nuclei per 100,000 $\mu m^3$ and the dorsal SCN contained 23 nuclei per 100,000 $\mu m^3$ (Fig. 3d).

For the nuclei that were considered more than 50% but not 100% within our data set, we

observed that the ventral SCN contained 9 nuclei per 100,000 $\mu m^3$ and the dorsal SCN contained

15 nuclei per 100,000 $\mu m^3$ (Fig. 3d). For the neurons whose nuclei were less than 50% within

our data set, we observed that the ventral data set contained 23 nuclei per 100,000 $\mu m^3$ and those

of the dorsal SCN were 43 nuclei per 100,000 $\mu m^3$ (Fig. 3d). For a better comparison of the

density that the neurons occupy in each region, the total number of nuclei counted was added and divided by the respective region volume in which the analysis was made (Fig. 3c). The ventral SCN contains a total of 55 nuclei per 100,000 $\mu m^3$ and the dorsal SCN contains 82 nuclei per 100,000 $\mu m^3$ (Fig. 3c).

**Larger number of stigmoid bodies in the dorsal SCN compared to the ventral region**

We created a grid-based system and counted the total number of stigmoid bodies in each of the ventral and dorsal SCN sets. The total number of stigmoid bodies was divided by the respective volumes and then multiplied by 100,000 $\mu m^3$ for a better comparison of the numbers. In the ventral SCN, there were about 10 stigmoid bodies per 100,000 $\mu m^3$ whereas in the dorsal SCN there were about 28 stigmoid bodies per 100,000 $\mu m^3$ (Fig. 4). There was a greater number of stigmoid bodies in the dorsal SCN.

**Myelinated Axon innervate the SCN core more densely than the SCN shell**

Comparison between the number and percentage of innervation of myelinated axons in each of the dorsal and ventral SCN regions was done and quantified. The dorsal SCN received approximately 37 axonal innervations per 100,000 $\mu m^3$ and the ventral SCN received about 48 axonal innervations per 100,000 $\mu m^3$ (Fig. 5c). In addition, the total length of the myelinated axons that innervated each of the regions was calculated. Those axons innervating the ventral region were 2089.5 $\mu m$ total in length. The myelinated axons innervating the dorsal region were 1254.8 $\mu m$ total in length (Fig. 5b). The frequency of branch points for the myelinated axons was also determined in the two regions. Those innervating the dorsal SCN had no (zero out 53 total myelinated axons) branching whereas a few (4 out of a total of 85 counted myelinated axons) of those innervating the ventral SCN had a branch point (Fig. 5d).

**Higher percentage of proximal dendrites in the dorsal SCN compared to ventral SCN.**

In addition to counting the number of nuclei in each of the SCN regions, a comparison of the number of proximal dendrites was done for each region. This was done to get an estimate of the diversity with which the dendrites project to their own region compared to other regions. It was observed that the dorsal SCN contained more proximal dendrites compared to the ventral SCN. Out of the 211 sampled dendrites, 17% of them are proximal dendrites in the ventral SCN and 23% of them are proximal in the dorsal SCN (Fig. 6).

**No difference in the distribution of astrocytes across the two SCN regions**

For a thorough comparison of the ventral and dorsal SCN density, the number of astrocytes were counted in each region. The total number of astrocytes per region was then divided by the volume of the segmented area and then multiplied by 100,000 $\mu m^3$. A total of 7 astrocytes per 100,000 $\mu m^3$ was counted for each region (Fig. 7).

DISCUSSION

The core and the shell regions of the suprachiasmatic nucleus (SCN) are believed to control different circadian rhythm functions. In addition to looking at structural differences between the two regions, we looked to see if there are morphological differences between the two regions based on the innervations that they receive. mRGCs connect to cells in the SCN through swellings along their axons called boutons, which transmit information from the axon to the dendrite. An indication of synaptic strength is in number and size of boutons with which mRGCs make connections with cells in the SCN. Hence, bouton size and synaptic density may provide an insight into the strength of connections that the mRGCs make within the SCN and therefore, the intensity of the communication between the two cell types. It was observed that the mRGCs innervating the dorsal SCN contain higher density of boutons and are more branched than those that innervate the ventral SCN (Fig. 2). On average, the dorsal mRGC axon lengths are shorter than those in the ventral SCN (Fig. 2). This may indicate that the mRGCs innervating the dorsal SCN make more connections and their connections are more diverse, as the shorter length of the axon and increased degree of branching indicate more synaptic contacts are being made. Furthermore, the shorter length of the axons innervating the dorsal SCN may be due to the fact that the data set for the dorsal SCN was smaller than that of the ventral SCN which means that the axons captured in our data set may not be the full length or the true length of an mRGC axon.

We also saw that bouton volumes were on average larger in the dorsal SCN compared to the ventral SCN (Fig. 1). Larger boutons may indicate that the synaptic connection is stronger between the axon and the dendrite. More information regarding the number of vesicles present at the synaptic cleft is necessary for a better indication of the synaptic strength (Karunanithi et al.

2002). In addition, further analysis of the number of synaptic partners of mRGC boutons with the post-synaptic cells is an indication of how widely the signal is spread in each region.

We also observed that there were more mRGC boutons in the ventral SCN compared to the dorsal SCN (Fig. 1). The larger bouton density of mRGCs in the ventral region indicates that this region receives more innervations from the retina. Previously, it was shown that the ventral SCN receives most of the projections from the retina and that it projects to the dorsal SCN (Van den Pol and Tsujimoto, 1985). The data shown here supports the claim that the ventral region does receive more projections from the retina, however the dorsal region of the SCN also receives projections with mRGCs boutons of larger volume, indicating that the mRGCs may be making stronger synaptic connections with multiple partners in the dorsal region. A further step in the process of analysis of the synaptic strength of the mRGCs with SCN neurons is to quantify the number of synaptic partners each of the mRGC boutons make in the dorsal SCN. Based on our comparisons and previous research, synaptic strength is not solely dependent on bouton volume of mRGC axons, but also depends on the number of synaptic partners made and the density of the boutons in each region.

Although the results indicate that the mRGCs send larger quantity of synaptic boutons into the ventral SCN, it is still unknown whether all the dendrites that the mRGCs connect to in the ventral region belong in their respective region. For example, the dorsal SCN may have its dendrites passing through the ventral and it is in this region that the mRGCs make their connections. To determine whether the mRGCs are making their contacts with neurons that belong to the ventral or dorsal, the dendrites were skeletonized to determine which ones are proximal and which ones are distal. A quantification of proximal dendrites will indicate the dendrites that belong to the region that they are found in and distal dendrites will indicate that

they belong to another region. We have quantified the percentage of proximal dendrites per SCN region. In the ventral SCN we observed fewer percentage of proximal dendrites (Fig. 6), indicating that the neurons in the ventral SCN make fewer connections among themselves and they project mostly outward to other regions, when compared to the dorsal SCN. Additionally, from our observations (Fig 3) we saw that the dorsal region of the SCN is more densely packed with SCN neurons. Previously, Moore and colleagues have shown that the percentage of neurons in the dorsal SCN is 57% of total SCN neurons and that the ventral SCN contains 43% of total SCN neurons (Moore, 2002). Our results support this observation, and this may explain the larger percentage of proximal dendrites found in the dorsal SCN, since more neurons are present in this region. The greater percentage of proximal axons in the dorsal SCN is a sign that the dorsal neurons make more contacts within the region, however an analysis of the dendrodendritic chemical synapses (DDCS) is necessary to make such a conclusion of whether these synapses exist. Furthermore, based on these numbers and the percentage of connections observed from the mRGCs, the dense dorsal SCN may receive fewer projections from the retina through the mRGCs.

Further analysis of mRGC connections with cells of the SCN will offer insight into how different the two regions are. Thus far we see differences in morphology of the mRGCs that innervate the two regions however, we lack data about which cells types in the SCN they contact and where specifically on the neuron they make the majority of their contacts. Analyzing the specific contacts between the mRGCs and the SCN neurons will allow for a better understanding of their connectivity and it will help in developing mRGC specific drugs for treatment of circadian rhythm problems.

We also observed nuclei that resembled a neuronal nucleus, but they belonged to astrocytes. We counted the astrocytes separately and accounted for their numbers when analyzing the density of the neuron. There were equal numbers of astrocytes in each region (Fig. 7). In the SCN, astrocytes play a key role in the control of circadian rhythms. These cells express clock genes and their circadian rhythm is independent of neurons in the SCN (Prolo 2005). When Prolo et al., ablated the clock gene in the astrocytes, they noticed that the clock period of the mouse circadian rhythm was shorter. Further investigation of astrocytic dendrites and their synaptic connections is necessary to understand how they regulate the circadian rhythms. A limitation to this project is that astrocytic dendrites are thin, making it hard to capture their synaptic connections.

In addition to observing the innervation to the SCN from the mRGC axons, we also looked at innervations from myelinated axons. These axons are not projecting from the retina and are not mRGCs, as the mRGCs that project to the SCN are mostly unmyelinated. Our results indicate that the ventral SCN appears to contain more myelinated axons compared to the dorsal SCN. Since these axons were observed to not be making any synaptic connections with the neurons or cells in either SCN region, it is not clear if they are only passing through and connecting to different regions, or that we were unable to capture their connections in our limited SCN volume.

Further steps in analyzing the structural anatomy of the SCN would be to use transgenic mice with VIP and AVP cre recombinase targeted EM tags. This way the neurons of the SCN can be tagged at the same time as the mRGC ones and an analysis of the other projections innervating these regions can be done. To identify and differentiate the specific neurons in the SCN that the mRGCs connect it, we may need to use multiple genetic tags. Currently, we are

unable to determine if the mRGCs are making their connections with neurons of the ventral region or neurons of the dorsal region because the ventral region may send its dendrites to the dorsal region and we capture the mRGC connections in the dorsal, resulting in the data that identifies them as connections in the dorsal.

The data from this study has provided insight into the diversity of mRGC axons and the structural differences between the ventral and dorsal regions of the SCN. From this study, we know that the ventral and dorsal regions of the SCN receive innervation from the retina which is contrary to what was believed previously. Finally, further data collection will provide a clearer image of the structural anatomy of the SCN core and shell.
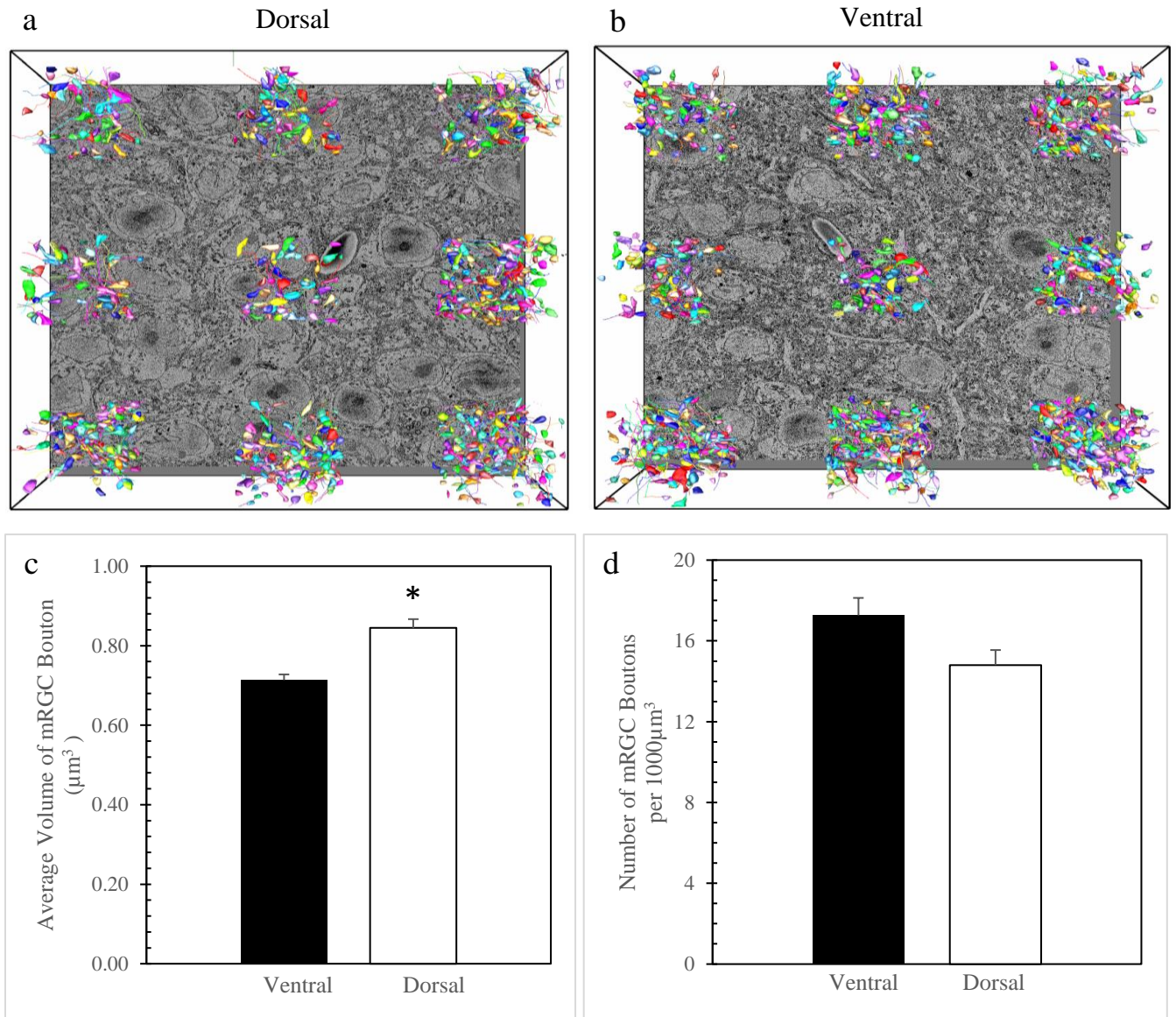
Figure 1. Average volume and density of mRGC boutons in the dorsal and ventral SCN. (a) Representative bouton from dorsal SCN. Scale bar is 2µm. (b) Representative bouton from ventral SCN. Scale bar is 2µm. (c) Average mRGC bouton volume in the dorsal and ventral SCN. Filled bar represents average bouton volume of ventral SCN and unfilled bar represent those in the dorsal SCN. Ventral mRGC bouton number count is 1063 and average bouton volume is 0.71µm$^3$. Dorsal mRGC bouton count is 677 and the average bouton volume is 0.84µm$^3$. Performed student t-test (p = 8.0x10$^{-07}$). (d) Density of mRGC boutons in the dorsal and ventral SCN. Density of mRGC boutons in the ventral SCN is 17.26 boutons per 1000µm$^3$ and those in the dorsal SCN are 14.81 boutons per 1000 µm$^3$.
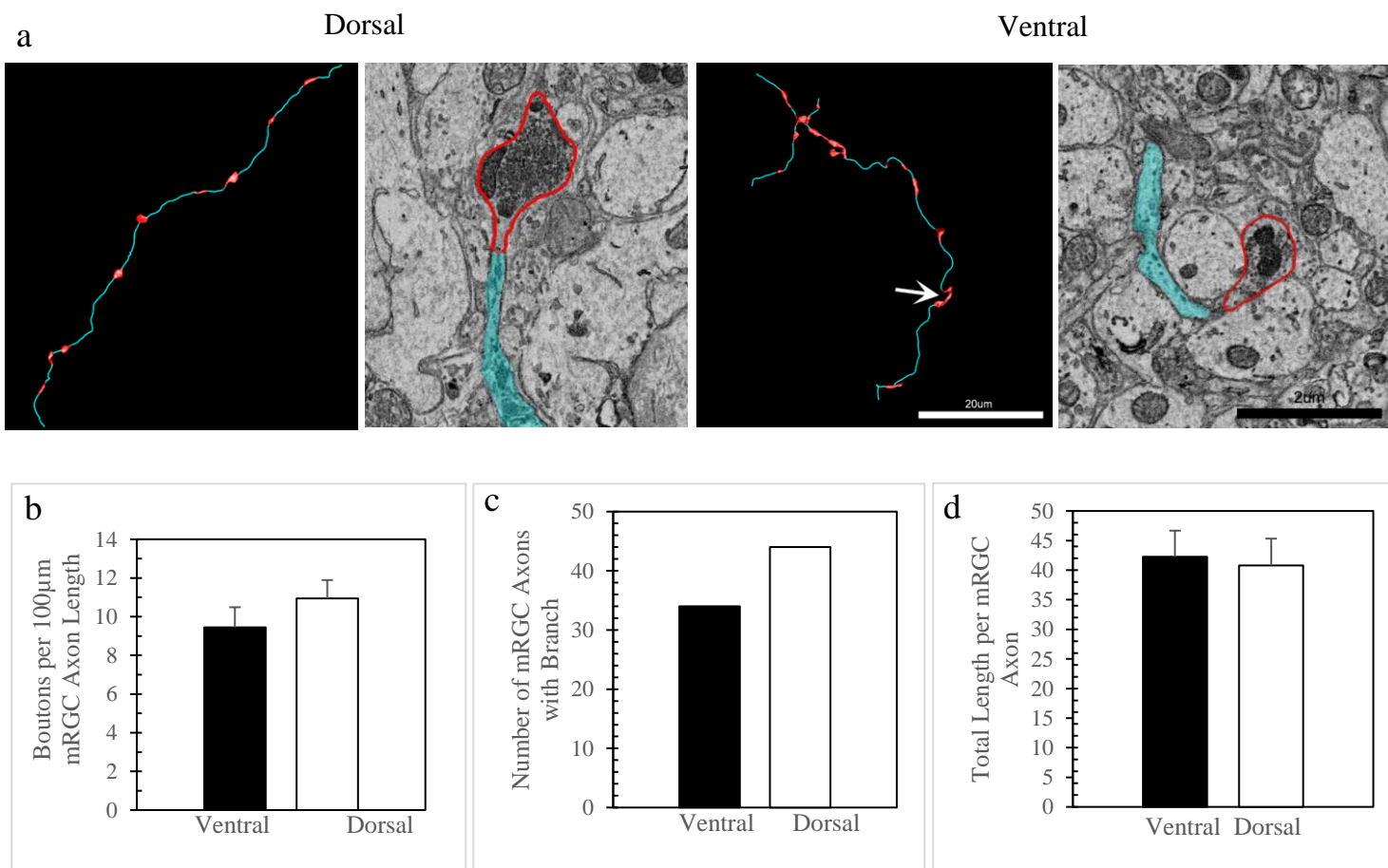
Figure 2. mRGC axon characteristics in the ventral and dorsal regions of SCN. Filled bars represent the ventral region of the SCN and open bar represents the dorsal region. Sampled 50 mRGC axons. (a) Boutons along the length of an axon from the dorsal and ventral regions. (b) Number of boutons per 100 µm mRGC axon length. 9.4 boutos per 100 µm length of axon in the ventral region and 10.9 boutons per 100 µm axon length in the dorsal region. No significant different in frequency of boutons; t-test (p = 0.29). (c) Percentage of mRGC axons with branch points. The ventral SCN had 34 out of 50 of its axons with a branch points and the dorsal SCN had 44 out of 50 of its axons with a branch point. (d) Total length per mRGC axon. Added the total length, including the branching points. The average length of an axon in the ventral SCN is 42 µm and that in the dorsal SCN is 40 µm. Error bars represent standard error of mean.
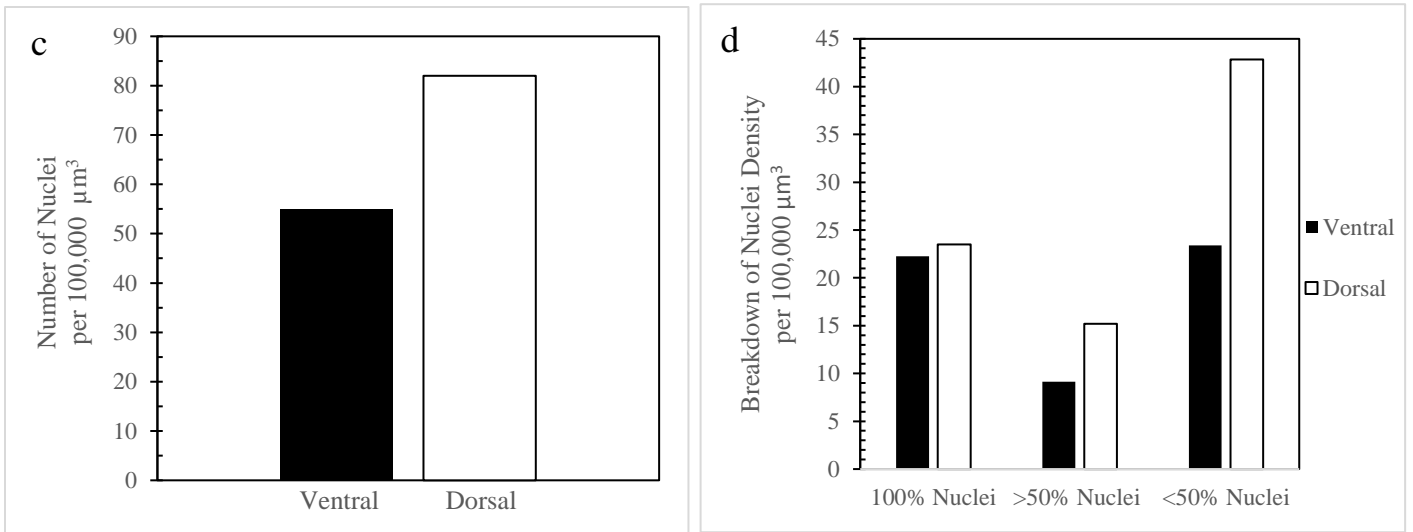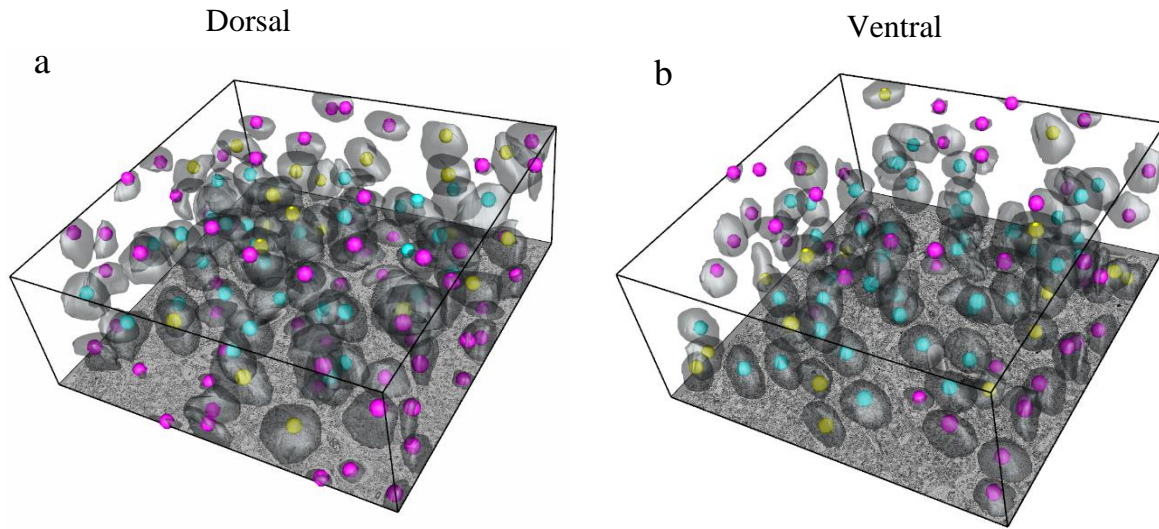
Figure 3. Density of nuclei in the ventral and dorsal SCN. Total number of nuclei in the dorsal and ventral SCN were counted and divided by the respective volume of the data set analyzed. The number was then multiplied by 100,000 $\mu m^3$ for normalization. (a) Total volume representation of nuclei within the dorsal SCN. (b) Volume representation of nuclei within the ventral SCN. (c) Total number of SCN nuclei counted and (d) is a breakdown of the nuclei number depending on whether it was fully contained (blue) within our data set or more than 50% (yellow) of it was included or less than 50% (pink) of it was within our data set. The ventral SCN had fewer nuclei overall, 55 nuclei per 100,000 $\mu m^3$ compared to 82 nuclei per 100,000 $\mu m^3$ in the dorsal SCN, indicating that it was less dense than the dorsal.
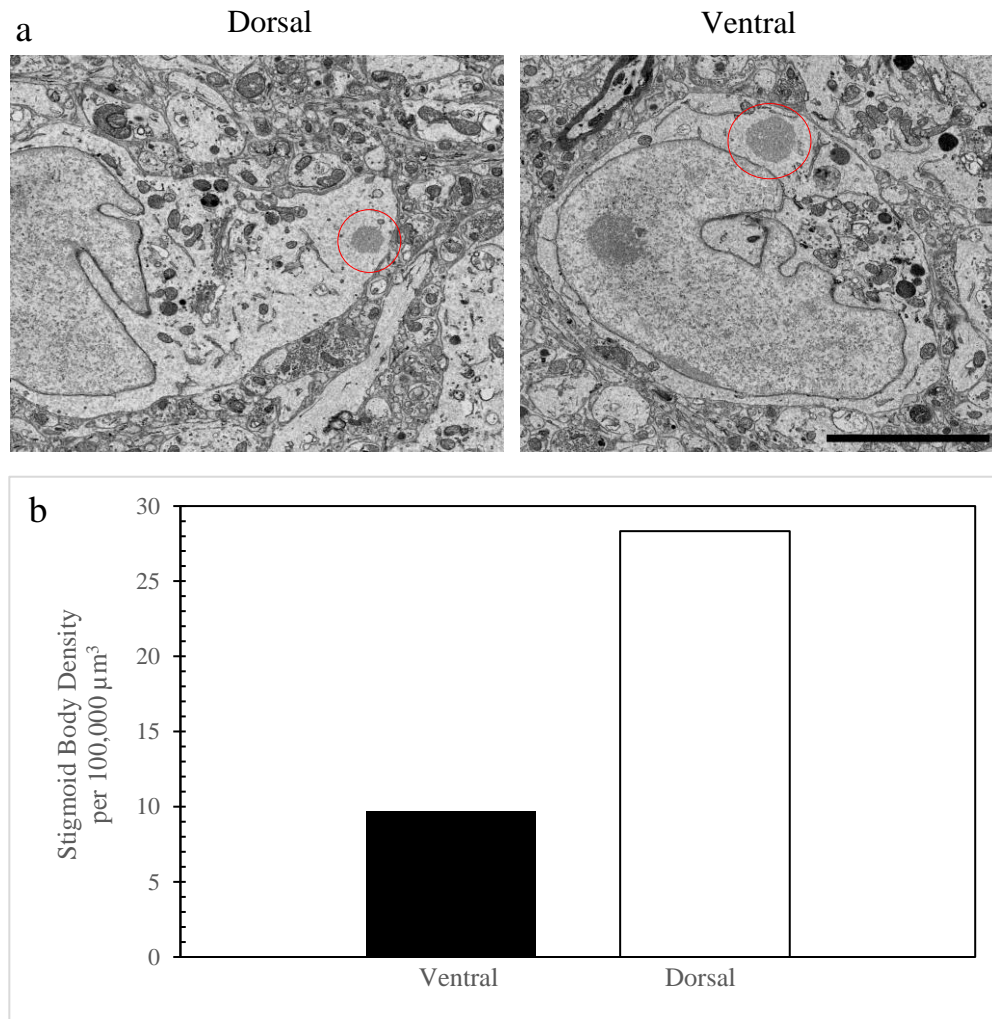
Figure 4. Fewer stigmoid bodies in the ventral compared to the dorsal region of the SCN. Manually counted all of the stigmoid bodies inside the data sets and divided by the respective volume of each data set. (a) Red circles represent the stigmoid bodies that are found in the cytoplasm of a neuron. (b) Bar graph representing the number of stigmoid bodies in each of the ventral and dorsal SCN. Filled bar graph represents the ventral region and unfilled graph is the dorsal. There are about 10 stigmoid bodies per 100,000 $\mu m^3$ in the ventral SCN and about 28 stigmoid bodies per 100,000 $\mu m^3$ in the dorsal SCN. Scale bar is 2 $\mu m$.
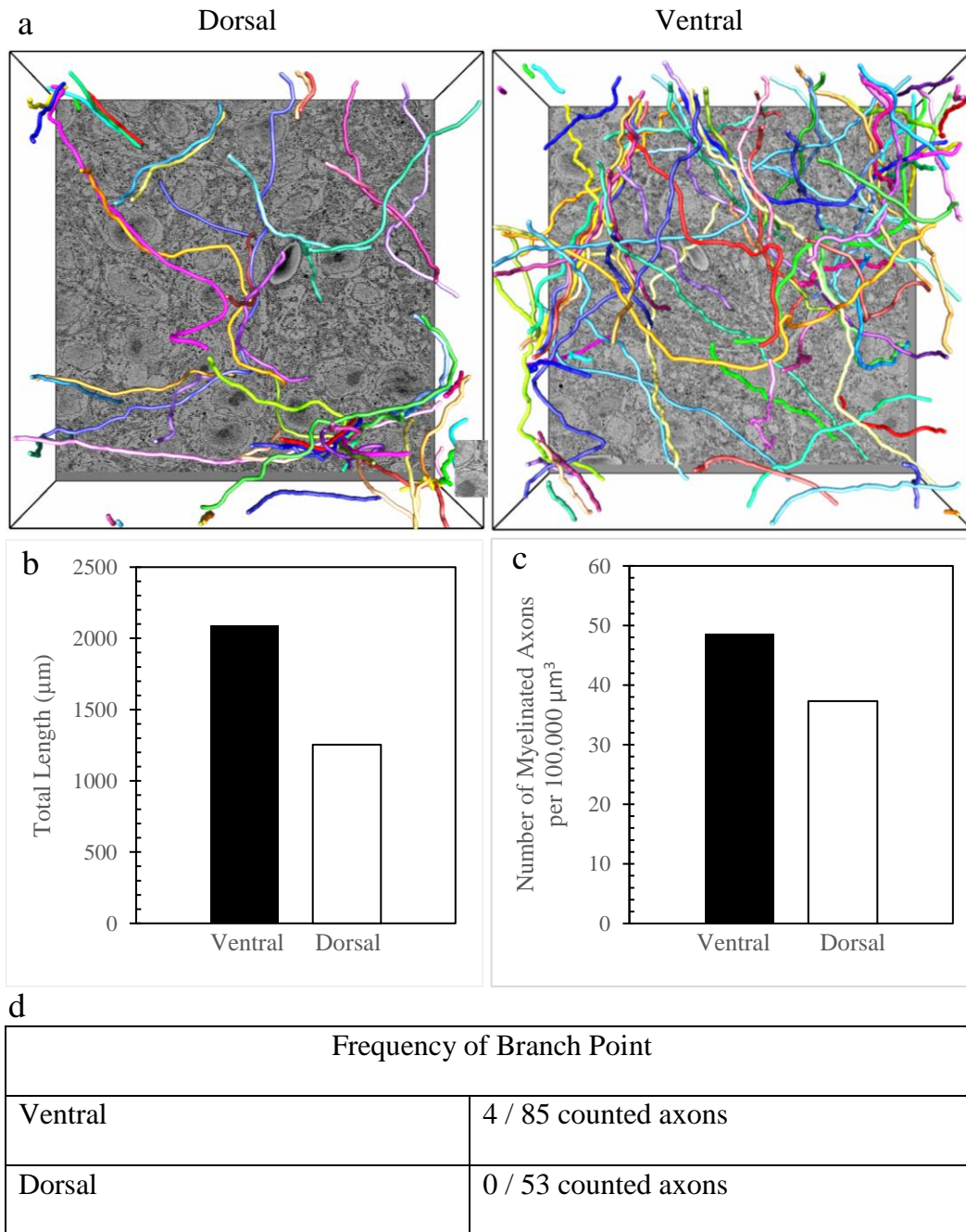
Figure 5. Myelinated axons project more densely to the ventral SCN compared to the dorsal SCN. (a) Representative images of the myelinated axons innervating the dorsal and the ventral SCN. (b) Total length of myelinated axons that project to each of the dorsal and ventral SCN. Filled bars represent the ventral region whereas unfilled bars represent the dorsal region. Total length of myelinated axons in the ventral SCN is 2,089.5 μm, and those innervated the dorsal SCN is 1,254.8 μm in total. (c) The ventral SCN is denser with myelinated axons with a count of 48 axons per 100,000 $\mu m^3$ compared to 37 axons per 100,000 $\mu m^3$ in the dorsal SCN. (d) Table representing the frequency of branch points of myelinated axons compared in the two regions. In the ventral there were a 4 out of the 85 found axons that contained multiple branches. There were no branches in the axons innervating the dorsal SCN.
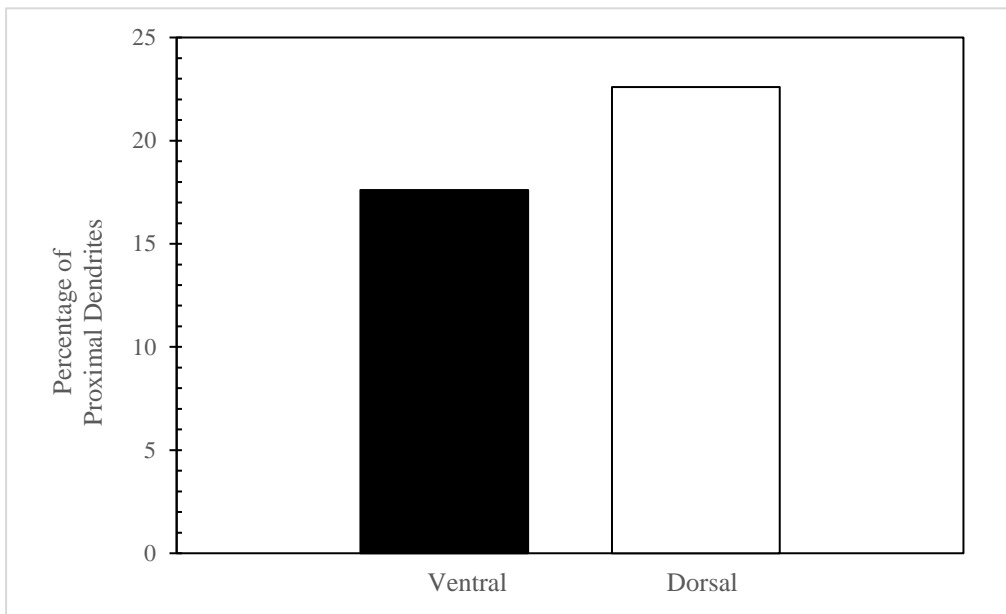
Figure 6. Dorsal SCN consist of more proximal dendrites. Randomly selected dendrites from a 10x10 grid and traced the dendrites to determine if they were proximal or distal. The number of dendrites that were proximal were then divided by the total number of dendrites traced per SCN region. Ventral SCN had about 17% proximal dendrites and the dorsal SCN about 22%.
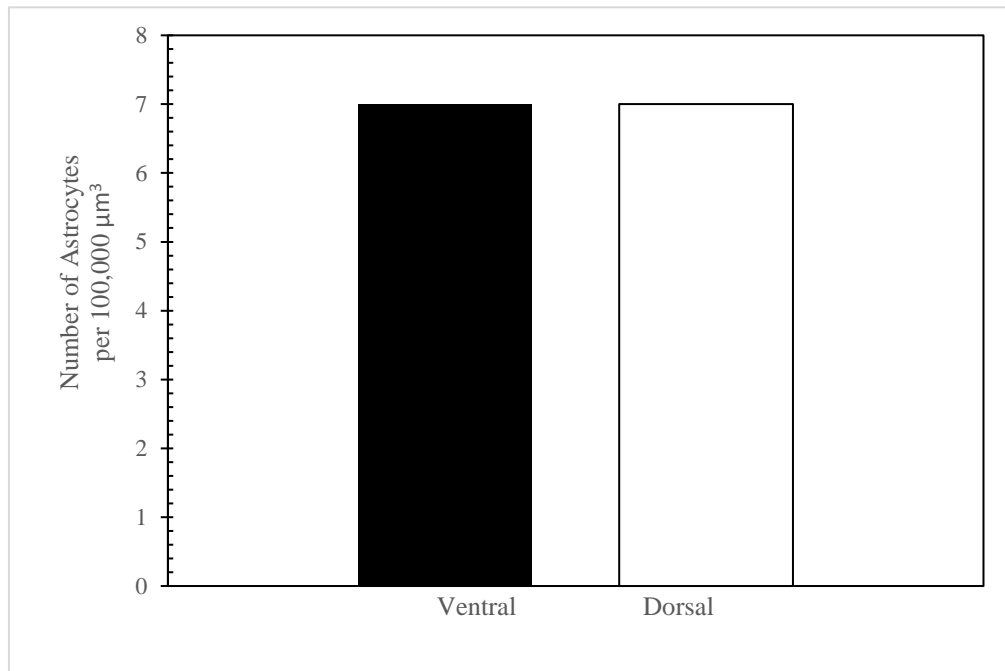
Figure 7. Number of astrocytes in the dorsal and ventral SCN. Filled bar graph represents the ventral region of the SCN and unfilled bar graph represents the dorsal region of the SCN. Normalization was done so that the numbers were comparable. There were about equal numbers of astrocytes in both the dorsal and the ventral SCN, 7 astrocytes per 100,000 $\mu m^3$ in both dorsal and ventral SCN regions.

REFERENCES

Abrahamson, Eric E., and Robert Y. Moore. 2001. "Suprachiasmatic Nucleus in the Mouse: Retinal Innervation, Intrinsic Organization and Efferent Projections." *Brain Research* 916 (1–2): 172–91. doi:10.1016/S0006-8993(01)02890-6.

Aschoff, Jürgen. 1965. "Circadian Rhythms in Man." *Science*. doi:10.1126/science.148.3676.1427.

Aton, Sara J., and Erik D. Herzog. 2005. "Come Together, Right...Now: Synchronization of Rhythms in a Mammalian Circadian Clock." *Neuron*. doi:10.1016/j.neuron.2005.11.001.

Berson, D.M., F.A. Dunn, and M. Takao. 2002. "Phototransduction by Retianl Ganglion Cells That Set the Circadian Clock." *Science* 295 (February): 953–59.

Denk, Winfried, and Heinz Horstmann. 2004. "Serial Block-Face Scanning Electron Microscopy to Reconstruct Three-Dimensional Tissue Nanostructure." *PLoS Biology* 2 (11). doi:10.1371/journal.pbio.0020329.

Ecker, Jennifer L., Olivia N. Dumitrescu, Kwoon Y. Wong, Nazia M. Alam, Shih Kuo Chen, Tara LeGates, Jordan M. Renna, Glen T. Prusky, David M. Berson, and Samer Hattar. 2010. "Melanopsin-Expressing Retinal Ganglion-Cell Photoreceptors: Cellular Diversity and Role in Pattern Vision." *Neuron* 67 (1). Elsevier Ltd: 49–60. doi:10.1016/j.neuron.2010.05.023.

Gachon, F, E Nagoshi, S A Brown, J Ripperger, and U Schibler. 2004. "The Mammalian Circadian Timing System: From Gene Expression to Physiology." *Chromosoma*. doi:10.1007/s00412-004-0296-2.

Guldner, Fritz. 1976. "Cell and Tissue Synaptology of the Rat Suprachiasmatic Nucleus *" 4.

Hastings, Michael H., and Erik D. Herzog. 2004. "Clock Genes, Oscillators, and Cellular Networks in the Suprachiasmatic Nuclei." *Journal of Biological Rhythms* 19 (5): 400–413. doi:10.1177/0748730404268786.

Hattar, S. 2002. "Melanopsin-Containing Retinal Ganglion Cells: Architecture, Projections, and Intrinsic Photosensitivity." *Science* 295 (5557): 1065–70. doi:10.1126/science.1069609.

Herzog, Erik D., Joseph S. Takahashi, and Gene D. Block. 1998. "Clock Controls Circadian Period in Isolated Suprachiasmatic Nucleus Neurons." *Nature Neuroscience*. doi:10.1038/3708.

Karunanithi, Shanker, Leo Marin, Kar Wong, and Harold L Atwood. 2002. "Quantal Size and Variation Determined by Vesicle Size in Normal and Mutant Drosophila Glutamatergic Synapses." *The Journal of Neuroscience* 22 (23): 10267–76. doi:22/23/10267 [pii].

Kofuji, Paulo, Ludovic S. Mure, Logan J. Massman, Nicole Purrier, Satchidananda Panda, and William C. Engeland. 2016. "Intrinsically Photosensitive Retinal Ganglion Cells (MRGCs) Are Necessary for Light Entrainment of Peripheral Clocks." *PLoS ONE* 11 (12): 1–23. doi:10.1371/journal.pone.0168651.

Kornmann, Benoît, Olivier Schaad, Hermann Bujard, Joseph S. Takahashi, and Ueli Schibler.

2007. "System-Driven and Oscillator-Dependent Circadian Transcription in Mice with a Conditionally Active Liver Clock." *PLoS Biology*. doi:10.1371/journal.pbio.0050034.

Lam, Stephanie S., Jeffrey D. Martell, Kimberli J. Kamer, Thomas J. Deerinck, Mark H. Ellisman, Vamsi K. Mootha, and Alice Y. Ting. 2014. "Directed Evolution of APEX2 for Electron Microscopy and Proximity Labeling." *Nature Methods* 12 (1): 51–54. doi:10.1038/nmeth.3179.

Leak, Rehana K., J. Patrick Card, and Robert Y. Moore. 1999. "Suprachiasmatic Pacemaker Organization Analyzed by Viral Transynaptic Transport." *Brain Research* 819 (1–2): 23–32. doi:10.1016/S0006-8993(98)01317-1.

Mieda, Michihiro, Daisuke Ono, Emi Hasegawa, Hitoshi Okamoto, Ken ichi Honma, Sato Honma, and Takeshi Sakurai. 2015. "Cellular Clocks in AVP Neurons of the Scn Are Critical for Interneuronal Coupling Regulating Circadian Behavior Rhythm." *Neuron* 85 (5). Elsevier Inc.: 1103–16. doi:10.1016/j.neuron.2015.02.005.

Moore, R Y. 1995. "Organization of the Mammalian Circadian System." *Ciba Foundation Symposium* 183: 88-99; discussion 100-6. http://www.ncbi.nlm.nih.gov/pubmed/7656695.

Moore, Robert Y., and J. Patrick Card. 1994. "Intergeniculate Leaflet: An Anatomically and Functionally Distinct Subdivision of the Lateral Geniculate Complex." *Journal of Comparative Neurology*. doi:10.1002/cne.903440306.

Moore, Robert Y., Joan C. Speh, and Rehana K. Leak. 2002. "Suprachiasmatic Nucleus Organization." *Cell and Tissue Research* 309 (1): 89–98. doi:10.1007/s00441-002-0575-2.

Morin, L. P., and C. N. Allen. 2006. "The Circadian Visual System, 2005." *Brain Research Reviews*. doi:10.1016/j.brainresrev.2005.08.003.

Morin, Lawrence P. 2013. "Neuroanatomy of the Extended Circadian Rhythm System." *Experimental Neurology* 243. Elsevier Inc.: 4–20. doi:10.1016/j.expneurol.2012.06.026.

Nakamura, Wataru, Sato Honma, Tetsuo Shirakawa, and Ken Ichi Honma. 2001. "Regional Pacemakers Composed of Multiple Oscillator Neurons in the Rat Suprachiasmatic Nucleus." *The European Journal of Neuroscience*. doi:10.1046/j.0953-816x.2001.01684.x.

Noguchi, Takako, Kazuto Watanabe, Akihiko Ogura, and Sadao Yamaoka. 2004. "SHORT COMMUNICATION The Clock in the Dorsal Suprachiasmatic Nucleus Runs Faster than That in the Ventral" 20 (June): 3199–3202. doi:10.1111/j.1460-9568.2004.03784.x.

Pol, Anthony N. van den. 1980. "The Hypothalamic Suprachiasmatic Nucleus of Rat: Intrinsic Anatomy." *Journal of Comparative Neurology* 191 (4): 661–702. doi:10.1002/cne.901910410.

Prolo, L. M. 2005. "Circadian Rhythm Generation and Entrainment in Astrocytes." *Journal of Neuroscience*. doi:10.1523/JNEUROSCI.4133-04.2005.

Schmidt, Tiffany M., Shih Kuo Chen, and Samer Hattar. 2011. "Intrinsically Photosensitive Retinal Ganglion Cells: Many Subtypes, Diverse Functions." *Trends in Neurosciences*. doi:10.1016/j.tins.2011.07.001.

Shu, Xiaokun, Varda Lev-Ram, Thomas J. Deerinck, Yingchuan Qi, Ericka B. Ramko, Michael W. Davidson, Yishi Jin, Mark H. Ellisman, and Roger Y. Tsien. 2011. "A Genetically Encoded Tag for Correlated Light and Electron Microscopy of Intact Cells, Tissues, and Organisms." *PLoS Biology* 9 (4). doi:10.1371/journal.pbio.1001041.

Takahashi, Joseph S., Hee-Kyung Hong, Caroline H. Ko, and Erin L. McDearmon. 2008. "The Genetics of Mammalian Circadian Order and Disorder: Implications for Physiology and Disease." *Nature Reviews Genetics*. doi:10.1038/nrg2430.

Verstreken, Patrik, Cindy V. Ly, Koen J.T. Venken, Tong Wey Koh, Yi Zhou, and Hugo J. Bellen. 2005. "Synaptic Mitochondria Are Critical for Mobilization of Reserve Pool Vesicles at Drosophila Neuromuscular Junctions." *Neuron* 47 (3): 365–78. doi:10.1016/j.neuron.2005.06.018.

Welsh, David K. 2007. "Gate Cells See the Light." *Journal of Biological Rhythms* 22 (1): 26–28. doi:10.1177/0748730406297067.

Welsh, David K., Diomedes E. Logothetis, Markus Meister, and Steven M. Reppert. 1995. "Individual Neurons Dissociated from Rat Suprachiasmatic Nucleus Express Independently Phased Circadian Firing Rhythms." *Neuron* 14 (4): 697–706. doi:10.1016/0896-6273(95)90214-7.

Welsh, David K., Joseph S. Takahashi, and Steve A. Kay. 2010. "Suprachiasmatic Nucleus: Cell Autonomy and Network Properties." *Annual Review of Physiology* 72 (1): 551–77. doi:10.1146/annurev-physiol-021909-135919.